Available online at www.sciencedirect.com

ScienceDirect

Procedia Engineering 10 (2011) 3692–3707

Engineering Procedia

ICM11

Functional fatigue of shape memory wires under constant-stress and constant-strain loading conditions

G. Scirè Mammano[a] and E. Dragoni[a]

[a]*Dept of Engineering Sciences and Methods – University of Modena and Reggio Emilia Reggio Emilia – Italy*

Abstract

Shape memory alloys (SMAs) are increasingly used for the construction of simple solid-state actuators characterized by outstanding power density. The rational design of these actuators requires reliable data on the fatigue strength of the alloy under cyclic thermal activation (functional fatigue). The technical literature shows scanty test results for SMAs under functional fatigue. Furthermore, the few data available are mainly limited to the condition of constant stress applied to the material. Since the SMA elements used within actuators are normally biased by conventional springs or by another SMA element, their stress condition is far from constant in operation. The disagreement between actual working conditions and laboratory conditions leads to suboptimal designs and undermines the prediction of the life of the actuator. This paper aims at bridging the gap between experiment and reality. Four characteristic test conditions are envisioned, covering most of the actual situations occurring in practice: constant-stress, constant-strain, constant-stress with controlled maximum strain and cyclic-stress with controlled maximum strain. The paper presents the experimental apparatus specifically designed to implement the four test conditions. Fatigue results on a commercial NiTi wire (0.15 mm diameter) tested under constant-stress and constant-strain loading are also presented and discussed.

Keywords: SMA wires; functional fatigue; constant-stress loading; constant-strain loading

1. Introduction

Shape memory alloys (SMAs) are increasingly employed to build solid state actuators, characterized by sleek design and outstanding power density. For the rational design of shape memory actuators, a thorough knowledge of the fatigue behaviour of the alloy is needed [1]. Since the actuation is always provided by thermal activation of the alloy, the fatigue incurred by the material is called “thermomechanical” or “functional”, implying that material performs mechanical work against the external applied load when heated during the actuation cycle.

Although the purely mechanical fatigue (i.e. at constant temperature) of shape memory alloys is well established in the technical literature [2], only scanty data exist on the response of these materials to functional fatigue. The reason for this unbalance is due to the fact that shape memory alloys so far have been predominantly utilized for their superelastic behaviour (springs, dampers etc.) rather than for the shape memory effect (actuation). Furthermore, the few papers available on functional fatigue of shape memory alloys are limited to the constant-

1877-7058
Selection and peer-review under responsibility of ICM11 doi:10.1016/j.proeng.2011.04.607

stress loading condition and cover a very limited number of cycles. In [3,4] the functional fatigue of commercial SAES Getters SmartFlex® wires is presented. The wires are loaded by a constant stress (weight) and are cycled thermally by a suitable current supply. During the heating phase, the current is cut-off when the recovered displacement of the wire from the low-temperature position has achieved a pre-established value (partial transformation). The results of the fatigue tests in reference [3] are summarized in a diagram with applied stress and response strain plotted along the axes. Areas of the diagram are labelled with the minimum life expected for the corresponding combination of stress and strain levels. In [5], Bertacchini et al. investigated the functional fatigue under constant stress of shape memory wires by taking into account possible corrosion of the material. Eggeler [2] tested helical springs under constant external tensile forces, showing that both the spring length and the useful stroke increase with the number of cycles. In [6] Lagoudas et al. examined the functional fatigue of ternary NiTiCu wires with particular reference to the effect on the fatigue response of applied stress, annealing of the material and the degree of transformation of the alloy upon heating. In [7] Bigeon and Morin compared the functional fatigue behaviour of binary (NiTi) and ternary (CuZnAl) wires, showing that the shape memory effect is affected both by the applied stress and by the number of cycles. In particular, the effect of the number ob cycles is beneficial (training) and is more significant for the CuZnAl alloy. Bigeon and Morin followed up their functional fatigue tests in [8], highlighting a direct retaionship between the stress-assisted-two-way-memory-effect and the applied stress. They found that maximum recovery of the NiTi alloy was obtained for an applied stress of 200 MPa. In [9], a similar study is presented for TiNiCu wires and a Woehler-like curve linking applied stress to the number of cycles is proposed.

Nomenclature

A_f	Austenite finish temperature
A_s	Austenite start temperature
M_f	Martensite finish temperature
M_s	Martensite start temperature
N	Number of cycles
N_f	Number of cycles to failure
SME	Shape memory effect ($\equiv \Delta\varepsilon = \varepsilon_M - \varepsilon_A$)
S_0	Initial stress level
T	Temperature of wire
ε	Wire strain
ε_A	Wire strain in the austenitic state
ε_M	Wire strain in the martensitic state
ε_{max}	Maximum wire strain recorded in the cycle ($\equiv\varepsilon_M$)
ε_{min}	Minimum wire strain recorded in the cycle ($\equiv\varepsilon_A$)
$\Delta\sigma$	Stress variation recorded in the constant-stress cycle
ΔS	Stress increment used in the staircase method
σ	Wire stress
σ_w	Fatigue limit

Test methods different from the constant-stress concept were carried out in [10] and [11]. Mertmann et al. [10] investigated the stability of the shape memory effect under constant-strain conditions. They observe that memory effect is quickly lost under these conditions accompanied by a general elongation of the specimen. Demers et al. [11] tested the functional fatigue of a NiTi alloy after various thermomechanical training processes based on three steps: "stress-free shape recovery", "constrained recovery" (constant-strain) and "constant-stress recovery" (assisted-two-way-shape-memory-effect).

The difficulties faced by the designer of shape memory actuators are twofold. First, the commercial alloys available are unlikely to be covered by the test results retrieved from the literature. Second, the constant-stress loading condition behind the rare test results available are poorly representative of the true working conditions of the alloy in a real SMA actuator. This is because the backup force on the SMA element in an actuator is typically provided by a conventional spring or by another SMA element, which exert forces that are not constant. This discrepancy leads to suboptimal design and to the practical impossibility to predict the fatigue life of the device.

This paper aims at filling the gap between test conditions and working conditions of the shape memory materials in the context of functional fatigue. To this aim, a set of four different loading conditions are defined so as to meet closely the typical working conditions of real actuators: constant-stress, constant-strain, constant-stress with controlled maximum strain and cyclic-stress with controlled maximum strain. The paper presents the experimental apparatus purposely designed to achieve these test conditions and illustrates the fatigue results for commercial NiTi wires (Smartflex® 150) tested under constant-stress and constant-strain conditions.

2. Materials and methods

2.1. Characteristic stress-strain tests

Typically, a shape memory actuator comprises an active SMA element (for example a wire) and a backup element (for example a spring) used to restore the reference position when the SMA element is deactivated. The particular load acting on the active element strongly depends on the backup element and on the external load applied to the actuator. Apart from the very particular case of constant backup force and constant external load, the force on the active SMA element is not constant over the operating cycle but oscillates between a minimum and a maximum value, depending on the particular situation. If the end positions of the actuator are ensured by hard stops, the force on the active element is still variable but its strains are confined between a lower and an upper limit determined by the mechanical restraints. A limit case of this condition occurs when the SMA element is activated in a fully constrained position so that the stress varies at constant strain. This situation typically occurs in SMA devices used as static force generators [11], but it can arise also in actuators used to actuate grippers [10] or to displace high masses subject to strong accelerations. In the latter case, the loading conditions of the SMA element are close to a fixed-strain situation if the actuation time of the SMA is lower than the characteristic time of the inertial load [12]. Another situation of fixed-strain loading can occur when an external constraint locks the actuator in a fixed-position during the active stroke of the actuator.

Figure 1 illustrates four test conditions in which the stress and the strain in the SMA element vary along specific paths representative of what can occur in the operation of an actuator as described above.

Figure 1a describes the classical constant-stress test, in which the SMA element undergoes variable strain under prescribed stress, provided for example by an applied constant load. This test reproduces the situation occurring in an actuator backed up by a constant force and operated under no external load (positioning device). Given the material, this test is fully defined by the stress applied to the SMA element.

Figure 1b describes the constant-strain test, in which the SMA element undergoes variable stress under prescribed strain, provided for example by rigid restraints fixing the ends of the sample. This test reproduces the situation in which the actuator is operated in a locked position. Given the material, this test is fully defined by the strain imposed to the SMA element.

Figure 1c describes a constant-stress test with limited maximum strain, in which the SMA element undergoes variable strain under prescribed stress but the maximum strain achievable is limited by an external restraint. This test

reproduces the situation in which an actuator backed up by a constant force works between hard stops. Given the material, this test is fully defined by two parameters: the applied stress and the maximum strain.

Figure 1d describes a cyclic-stress test with controlled maximum strain, in which the SMA element undergoes variable strain under two-level constant stress. The stress level during activation of the material is higher than during deactivation and the maximum strain is again limited by an external constraint. This test reproduces the situation in which an actuator backed up by a constant force works against a constant dissipative load. Given the material, this test is fully defined by three parameters: the two stress levels and the maximum strain.

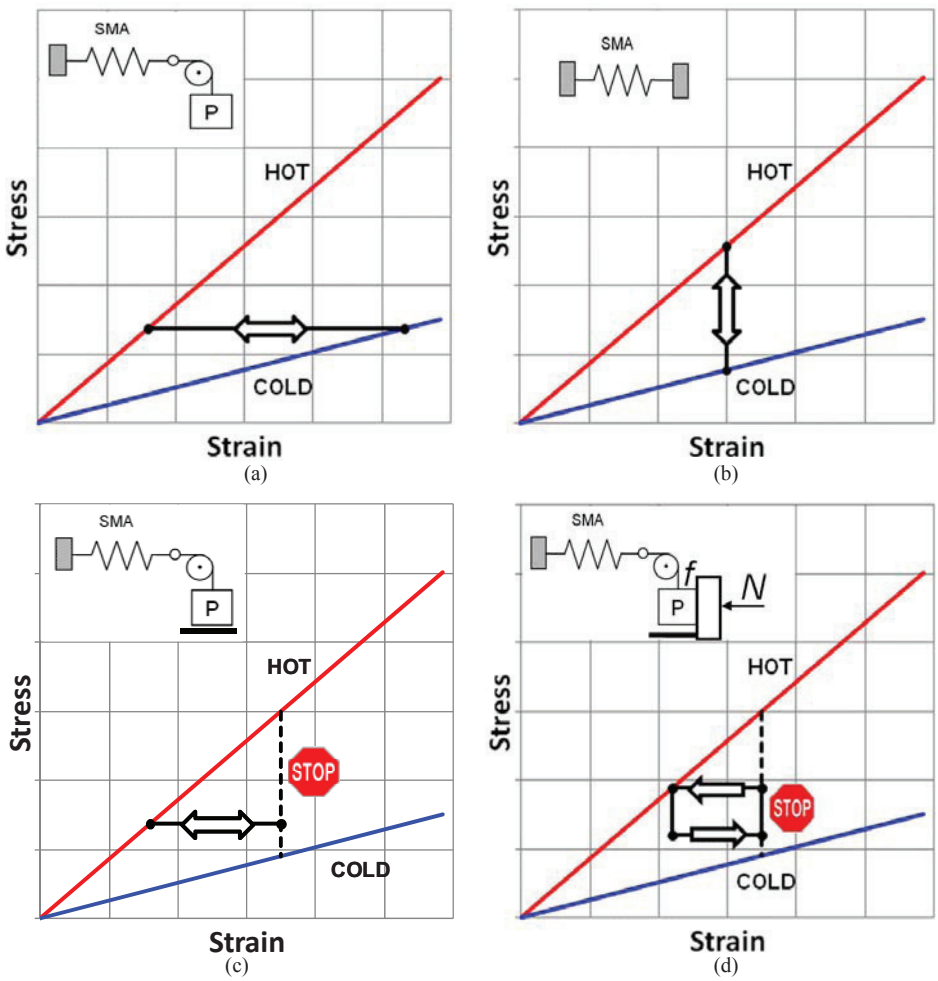

Fig. 1. Specific tests proposed to characterize the SMA wires under functional fatigue: (a) constant-stress, (b) constant-strain, (c) constant-stress with limited maximum strain, (d) cyclic-stress with controlled maximum strain

2.2. Experimental equipment

To apply the four stress-strain conditions in Section 2.1 to SMA wires, the test machine shown in Fig. 2 was built. The machine comprises a primary aluminium chassis to which a secondary plastic frame is attached. The upper part of the plastic frame holds the load cell (capacity of either 30 N or 250 N) to which one end of the SMA wire under test is attached through a rigid clamp.

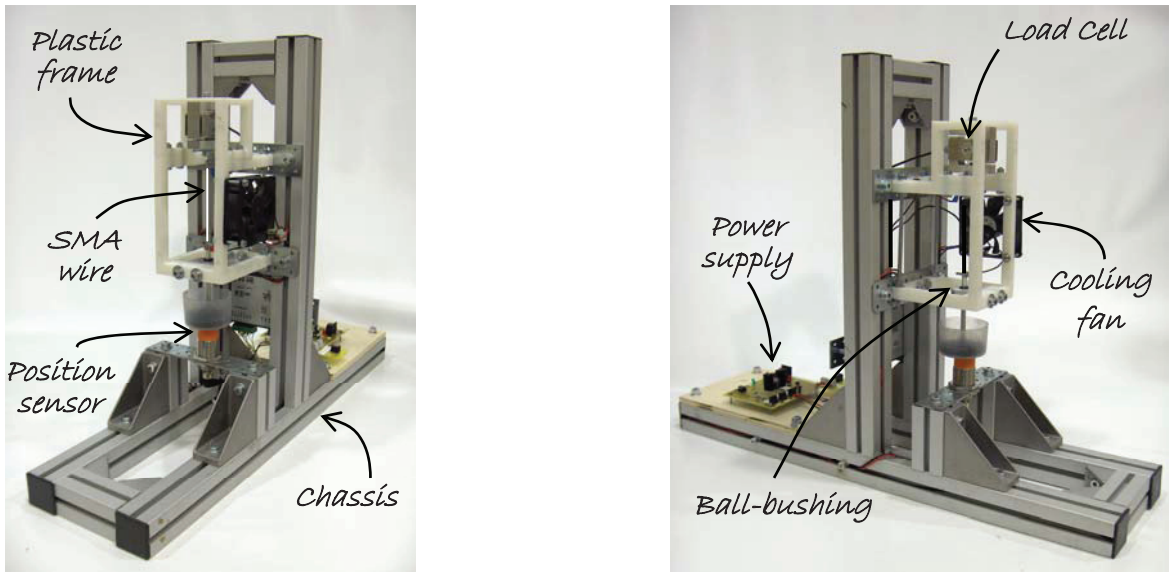

Fig. 2. Pictures of the testing machine used to characterize the SMA wires under the loading conditions shown in Fig. 1

The lower end of the SMA wire is attached to a vertical rod, guided by a ball bushing and equipped at the lower end with a basket containing the loading weight (small lead beads). The displacement of the basket is measured from below by an inductive position sensor (ifm electronic® II5914 with maximum range of 15 mm). Heating of the wire is provided by electric current supplied by an electronic power board. Cooling of the wire is enhanced by an electronically- controlled variable-speed fan.

In the configuration shown in Fig. 2 and detailed in Fig. 3a, the equipment can achieve the constant-stress stress conditions illustrated in Fig. 1a. By removing the lower basket and locking the bottom end of the rod as shown in Fig. 3b, constant-strain test conditions as in Fig. 1b can be obtained. By placing a polymer spacer on top of the displacement sensor to function as a hard stop for the loading basket (Fig. 3c), the test conditions in Fig. 1c (constant-stress with limited maximum strain) can be implemented. The test conditions in Fig. 1d (variable strain under two-level constant stress) can be achieved by equipping the machine with a friction device (not shown here), which acts on the supporting rod of the moving basket.

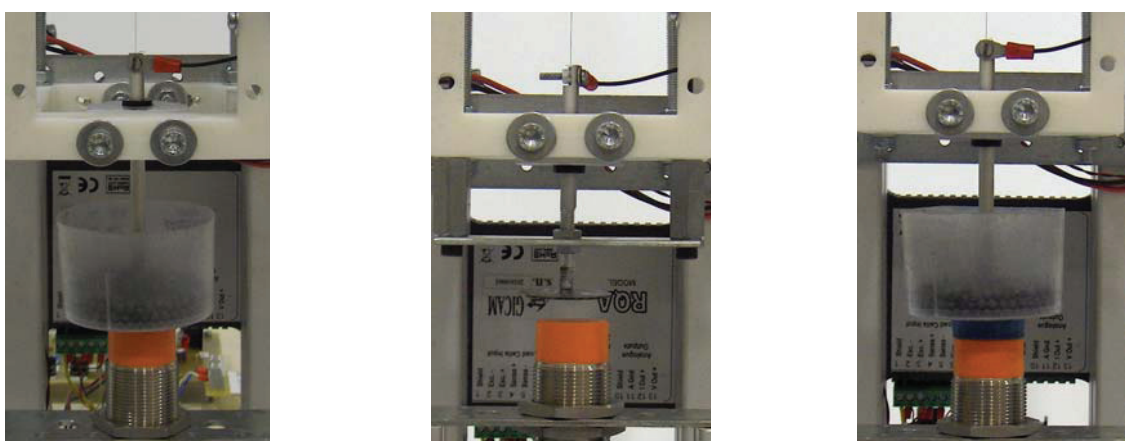

(a) (b) (c)

Fig. 3. Close-ups of the loading devices used to apply three of the loading conditions shown in Fig. 1: (a) constant-stress, (b) constant-strain, (c) constant-stress with limited maximum strain

The electronic power board is supplied through a linear voltage supplier with feedback on the current flowing in the wire. The supplied current and the signals from the sensors (load cell and displacement transducer) are picked up, processed and controlled by a DAQ board (National Instruments USB 6251). The operating parameters are displayed on the graphical user interface shown in Fig. 4 (LabView® application) and are stored in memory according to whatever acquisition scheme is requested by the user.

Fig. 4. Graphical user interface for setting-up, monitoring and controlling the fatigue tests

2.3. Properties of the tested shape memory alloy

This paper presents experimental results on SMA wires tested using the machine for the first two stress-strain conditions of Section 2: constant-stress and constant-strain. These two test conditions were chosen because they represent the limit conditions under which the SMA element can work within an actuator. Tests for the other two loading conditions have been planned and are under way.

To the aim of gathering fatigue data on shape memory materials readily available to the designer, the NiTi wire Smartflex® 150 marketed by SAES Getters was used throughout the experimental campaign. The wire has a diameter of 0.150 mm, a Ni content of 54% by weight and the following transformation temperatures: $A_s = 86°C$, $A_f = 94°C$, $M_s = 65°C$, $M_f = 57°C$.

Figure 5a shows the stress-strain tensile properties of the wire in the martensitic (solid circles) and austenitic (hollow circles) state. A detail of the martensitic curve is also shown in Fig. 5b. The tensile test was performed on a Galdabini Sun500 electromechanical machine operated at a strain rate of $1.67\times10^{-4}\ s^{-1}$. The austenitic transformation was achieved and maintained by supplying the wire with a steady current of 500 mA at room temperature.

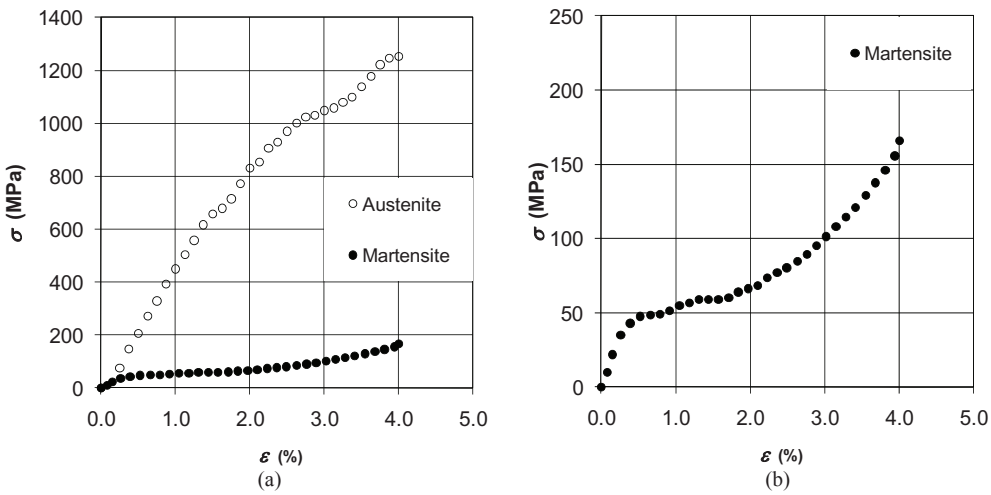

Fig. 5. Monotonic tensile stress-strain curves for the SMA wire tested (Saes Getters Smartflex®): (a) austenitic and martensitic curves; (b) detail of the martensitic response

2.4. Constant-stress tests

Testing procedure

Based on exploratory experiments, the constant-stress tests on the SMA wire were performed according to the following procedure:

1. a wire length of about 130 mm is cut from the coil
2. one end of the wire is attached to the load cell and the reading of the cell is set to zero
3. the free wire (no applied load) is heated above A_f to recover the memorized shape
4. the basket is attached to the other end of the wire (which is maintained above A_f) to achieve a test length of 100 mm
5. the reading of the displacement transducer is set to zero
6. the current supply is cut-off and the wire is let to cool down to room temperature
7. the basket is filled with lead beads until the desired stress in the wire (read by the load cell and displayed by the user interface) is reached
8. the test is started by supplying the wire with a sinusoidal current oscillating from zero to a peak value capable of producing the full transformation of the alloy under the cooling conditions adopted
9. the test is terminated automatically at fracture of the SMA wire (no current flowing in the sample) or when a prescribed number of cycles (5×10^5) have been endured with no failure.

By acting on the peak supply current and on the speed of the cooling fan, the test frequency in Step 8 above was kept as high as possible to reduce the test time. The maximum achievable frequency is limited by the force ripples in the wire produced by the inertia forces acting on the moving basket. All the tests were performed so that the actual stress in the wires was contained within 6% of the nominal stress (i.e. the stress produced by the pure weight of the basket with its content of lead beads). This requirement led to test frequencies ranging from 0.31 to 0.42 Hz and peak supply currents ranging from 0.83 to 1.04 A.

Stress levels

There is a strong similarity between the present constant-stress tests on SMA wires and the classical fatigue tests on ordinary construction materials. Both tests aim at identifying the number of cycles to failure for given applied stress (Woehler's strength-life curve). Due to this analogy, the fatigue data on the SMA wires were collected following the standard test method developed by the Japanese Society of Mechanical Engineers (JSME) [13]. The JSME method identifies Woehler's curve with as few as 14 tests, with 8 tests used to trace the inclined part of the curve and 6 used to calculate the horizontal part (fatigue limit).

Applied to the SMA wire under investigation, the JSME protocol produced the following stress levels at which the alloy had to be tested to identify the inclined part of the Woehler's curve: $S_0+3 = 225$ MPa, $S_0+2 = 200$ MPa, $S_0+1 = 175$ MPa, $S_0 = 150$ MPa, $S_0-1 = 125$ MPa, $S_0-2 = 100$ MPa, $S_0-3 = 75$ MPa. The tests begin at level S_0 and go on by stepping down one level at a time until one sample survives the test (no failure observed after 5×10^5 cycles). Further tests are then performed by stepping up one level at a time until two life results are obtained at each of the four levels above that at which no failure was observed. Using the fatigue data obtained for the inclined part of the curve, the method identifies a stress increment ΔS (equal to the standard deviation of the stress data gathered so far for the failed specimens) to be used in a final staircase method. In the staircase stage, the stress level of the next test is increased or decreased by ΔS according to whether the current test has produced a survival or a failure. The fatigue limit (for a probability of 50%) is computed as the average of the six stress levels of the staircase method.

2.5. Constant-strain tests

Testing procedure

After a series of exploratory trials, the constant-strain tests were performed according to the following procedure:

1. a wire length of about 130 mm is cut from the coil and copper eyelet terminals are crimped to both ends giving a net test length of 100 mm. (The use of crimps was necessary to avoid fractures under the clamps of the machine.)
2. one end of the wire is attached to the load cell and the reading of the load cell is set to zero
3. the free wire (no load applied) is heated above A_f to recover the memorized shape
4. the other end of the wire (which is maintained above A_f) is attached to the lower cross-head (see Fig. 3b)
5. the wire is slightly stretched (about 5 MPa) by means of the lower adjusting screws (Fig. 3b) and the reading of the displacement transducer are set to zero
6. the current supply is cut-off and the wire is let to cool down to room temperature
7. the prescribed strain (read by the displacement transducer and displayed by the user interface) is applied to the wire by lowering the cross-head in Fig. 3b
8. the test is started by supplying the wire with a sinusoidal current oscillating from zero to a peak value capable of producing the full transformation of the alloy under the cooling conditions adopted
9. the test is terminated automatically at fracture of the SMA wire (no current flowing in the sample) or when a prescribed number of cycles (5×10^5) have been survived.

For the constant-strain tests, high test frequencies were easier to achieve than for constant-stress tests because there was no inertia loads on the wire due to the moving. However, for similarity with the constant-stress tests, all the constant-strain experiments were performed at test frequencies ranging from 0.31 to 0.38 Hz. The supply currents needed to sustain these frequencies ranged from 1.12 to 1.22 A.

Strain levels

Similarly to the constant-stress tests, the constant-strain tests were aimed at determining the fatigue-life curve of the SMA in terms of cycles to failure as a function of the applied strain. Since generally recognized test schemes are not available for strain-controlled fatigue tests, the experimental plan adopted in the test campaign included five

strain values (1, 2, 3, 4 and 5%) with three samples per level. These five test strains were chosen so as to embrace the strain range that would occur in typical applications of the wire for actuation purposes.

3. Results

3.1. Constant-stress tests

Table 1 reports the experimental results obtained from the test campaign under constant-stress conditions. Each row in Table 1 corresponds to one of the 14 samples required by the JSME fatigue scheme described in Section 2.4. The nine tests 1-9 belong to the first part of the method, devoted to the identification of the inclined part of Woehler's curve. Test number 3 (applied stress of 100 MPa) corresponds to the lowest stress level during the first part of the method at which no failure (after 5×10^5 cycles) was detected. Test number 3 is the starting point of the final staircase method, including tests 10-13 as following steps. It is seen that the stress increment for the staircase method was $\Delta S = 11$ MPa.

The columns in Table 1 contain the applied stress (σ), the number of cycles survived (N_f), the percent stress oscillation measured during the test ($\Delta\sigma$), the minimum ($\varepsilon_{min} \equiv \varepsilon_A$), maximum ($\varepsilon_{max} \equiv \varepsilon_M$) and differential ($SME \equiv \Delta\varepsilon = \varepsilon_{max} - \varepsilon_{min}$) strains measured in the wire. The last four variables (from the stress oscillation, $\Delta\sigma$, to the differential strain, *SME*) are listed both for the second cycle after the start of the test and for the last cycle before test termination.

Table 1. Experimental results from the constant-stress fatigue tests (* = no failure observed)

			Second cycle after start				*Last cycle before termination*			
Test	σ (MPa)	N_f	$\Delta\sigma$ (%)	$\varepsilon_{min}\equiv\varepsilon_A$ (%)	$\varepsilon_{max}\equiv\varepsilon_M$ (%)	$\Delta\varepsilon\equiv SME$ (%)	$\Delta\sigma$ (%)	$\varepsilon_{min}\equiv\varepsilon_A$ (%)	$\varepsilon_{max}\equiv\varepsilon_M$ (%)	$\Delta\varepsilon\equiv SME$ (%)
1	150	9 688	3.8	0.50	4.93	4.43	4.4	1.01	5.39	4.38
2	125	25 901	4.4	0.47	4.64	4.17	4.5	0.72	4.84	4.12
3	100	500 000*	2.7	0.50	4.51	4.01	3.2	0.95	4.61	3.65
4	175	5 783	3.6	0.60	5.15	4.55	4.4	1.48	5.96	4.49
5	200	4 940	4.5	0.79	5.47	4.68	4.0	2.34	6.92	4.58
6	125	22 449	4.3	0.71	4.94	4.23	4.0	0.97	5.15	4.18
7	150	7 731	3.7	0.56	5.03	4.47	4.5	1.01	5.39	4.39
8	175	5 354	5.7	0.81	5.33	4.52	4.3	1.70	6.17	4.47
9	200	3 509	5.4	0.68	5.29	4.61	3.8	2.59	7.06	4.47
10	111	51 802	3.8	0.41	4.47	4.06	4.0	0.63	4.61	3.98
11	100	500 000*	4.6	0.60	4.54	3.94	3.0	1.02	4.64	3.62
12	111	32 923	4.1	0.36	4.49	4.13	4.3	0.53	4.50	3.97
13	100	389 614	3.2	0.47	4.40	3.93	3.4	0.84	4.45	3.61
14	89	500 000*	5.7	0.43	4.41	3.98	2.5	0.74	4.39	3.65

The data of applied stress (σ) and cycles to failure (N_f) from Table 1 are plotted in the semi-log Woehler diagram of Fig. 6 together with the interpolating lines obtained from the statistical elaboration of he results (Section 2.4). The equations of the interpolating lines are also provided.

Figure 7 shows the relationship between applied stress and corresponding strains (ε_{min}, ε_{max} and $\Delta\varepsilon$) induced in the wire in the second cycle afters test start (Fig. 7a) and in the last cycle before test termination (Fig. 7b).

For a selection of stress levels (σ = 100, 125, 150 and 200 MPa), Fig. 8 shows the trend of the characteristic strains as a function of the number of cycles endured by the wire.

Figure 9 shows the drift in the length of the martensitic wire as a function of the number of cycles. The drift is defined as the difference between the martensitic strain (ε_{max}) at the current cycle N and the martensitic strain measured in the second cycle. The drift parameter is a measure of the plastic strain accumulated by the wire during the tests.

3.2. Constant-strain tests

Table 2 reports the experimental results obtained from the test campaign under constant-strain conditions. The structure of this table is similar to Table 1 for the constant-stress tests, with the rows identifying the sample tested (three samples per strain level) and the following variables placed in the next columns: applied strain (ε), the number of cycles survived (N_f), the minimum (σ_{min}), maximum (σ_{max}) and differential ($\Delta\sigma = \sigma_{max} - \sigma_{min}$) stresses measured in the wire during the tests. The last four variables (from the minimum stress, σ_{min}, to the differential stress, $\Delta\sigma$) are listed both for the second cycle after the start of the test and for the last cycle before test termination.

The data of applied strain (ε) and cycles to failure (N_f) from Table 2 are plotted in the semi-log Woehler diagram of Fig. 10. The straight line drawn through the test points corresponds to the equation shown in the diagram, which was obtained by least-squares best fitting of the experimental points.

Figure 11 displays the maximum stress recorded in the second cycle after start and in the last cycle before test termination as a function of the applied strain.

Finally, Fig. 12 plots the maximum stress in the wire as a function of the number of cycles for all the 5 strain levels applied in the tests. The curves refer to the first sample tested at each level (see Table 2).

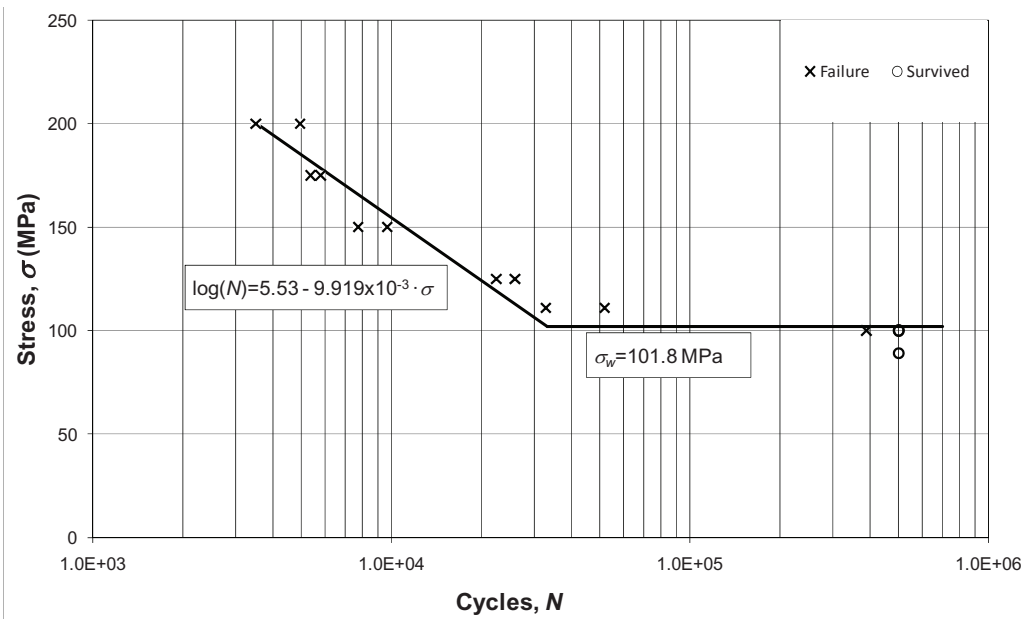

Fig. 6. Woehler's diagram with the fatigue results for the constant-stress test

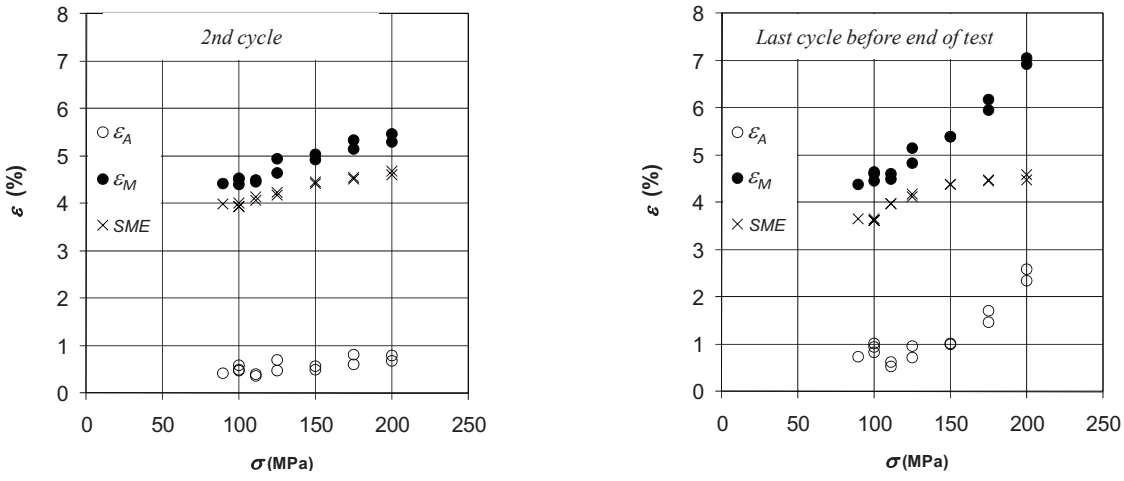

Fig. 7. Strains in the wire under constant-stress loading measured in: (a) the second cycle after test start; (b) the last cycle before test termination

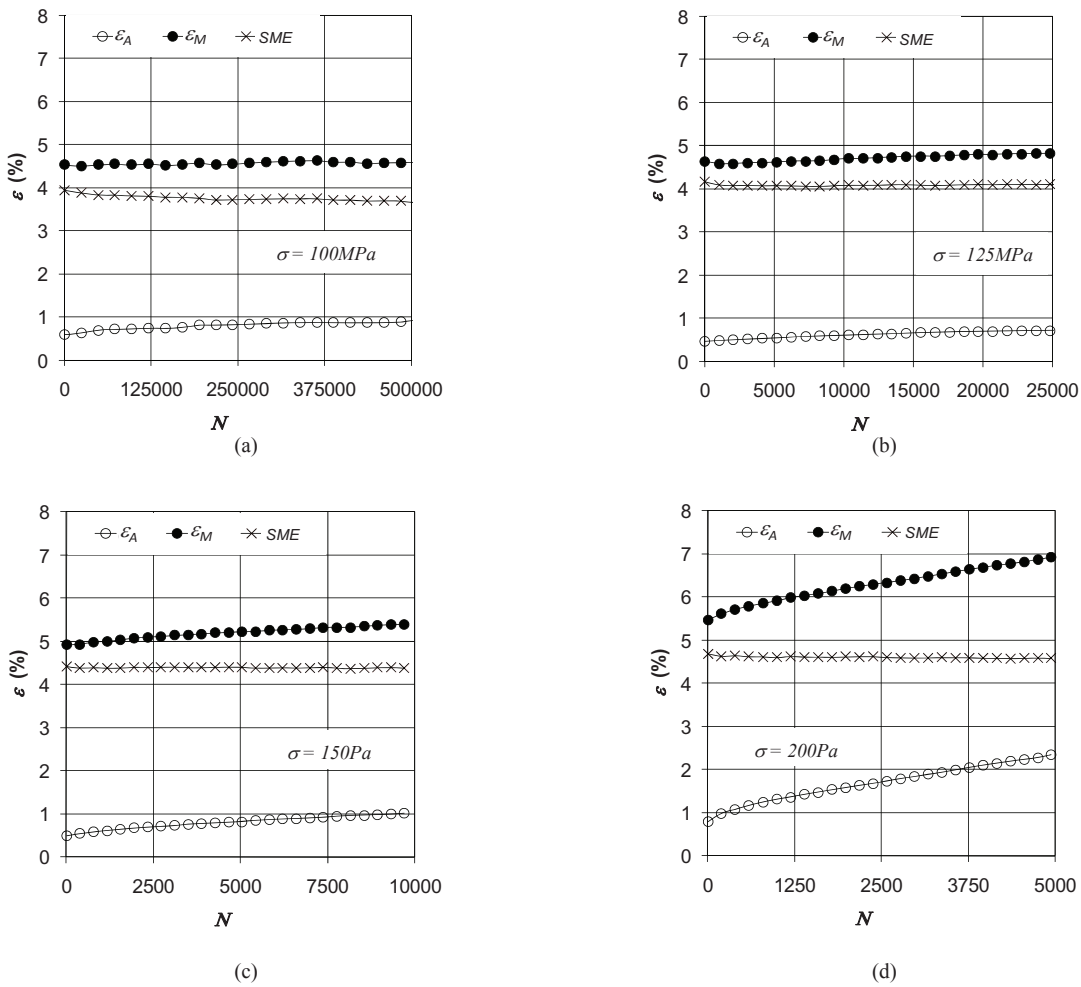

Fig. 8. Evolution of wire strains during the constant-stress tests: (a) 100 MPa; (b) 125 MPa; (c) 150 MPa; (d) 200 MPa

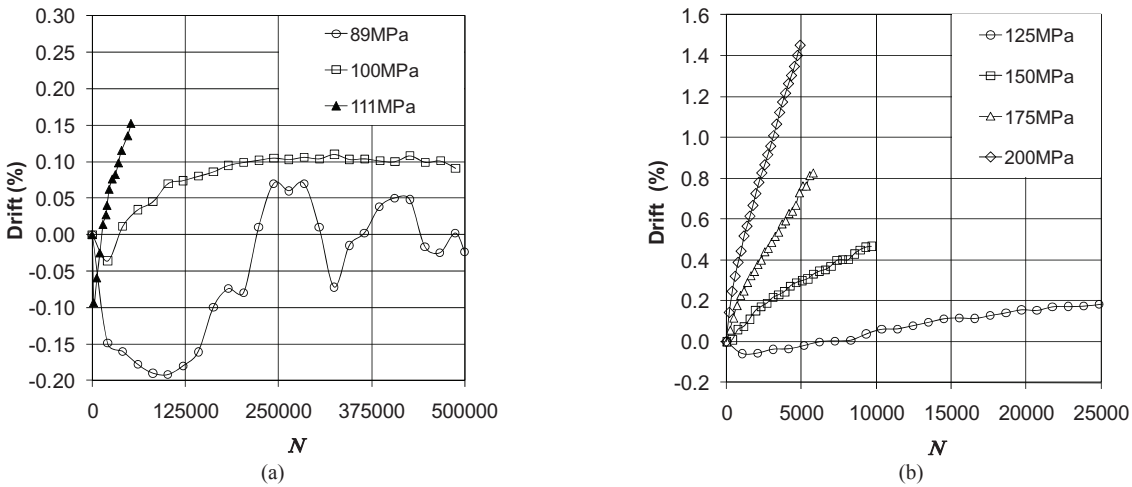

Fig. 9. Drift of martensitic wire length during the constant-stress tests: (a) low applied stress; (b) high applied stress

Table 2. Experimental results from the constant-strain fatigue tests

			Second cycle after start			*Last cycle before termination*		
Test	ε (%)	N_f	σ_{min} (Mpa)	σ_{max} (MPa)	$\Delta\sigma$ (MPa)	σ_{min} (Mpa)	σ_{max} (MPa)	$\Delta\sigma$ (MPa)
1	1	16.987	0	550	550	0	433	433
2	1	18.792	0	563	563	0	393	393
3	1	16.621	0	566	566	0	400	400
4	2	12.978	0	870	870	0	461	461
5	2	10.532	0	836	836	0	463	463
6	2	10.612	0	819	819	0	473	473
7	3	6.406	3	983	981	1	512	511
8	3	8.141	3	1044	1041	1	475	474
9	3	8.238	0	975	975	0	468	468
10	4	8.846	0	932	932	0	417	417
11	4	9.702	8	960	951	3	466	463
12	4	9.607	0	962	962	1	457	456
13	5	7.306	57	1025	968	37	490	453
14	5	7.056	27	1133	1106	24	425	401
15	5	7.159	31	1034	1003	4	415	412

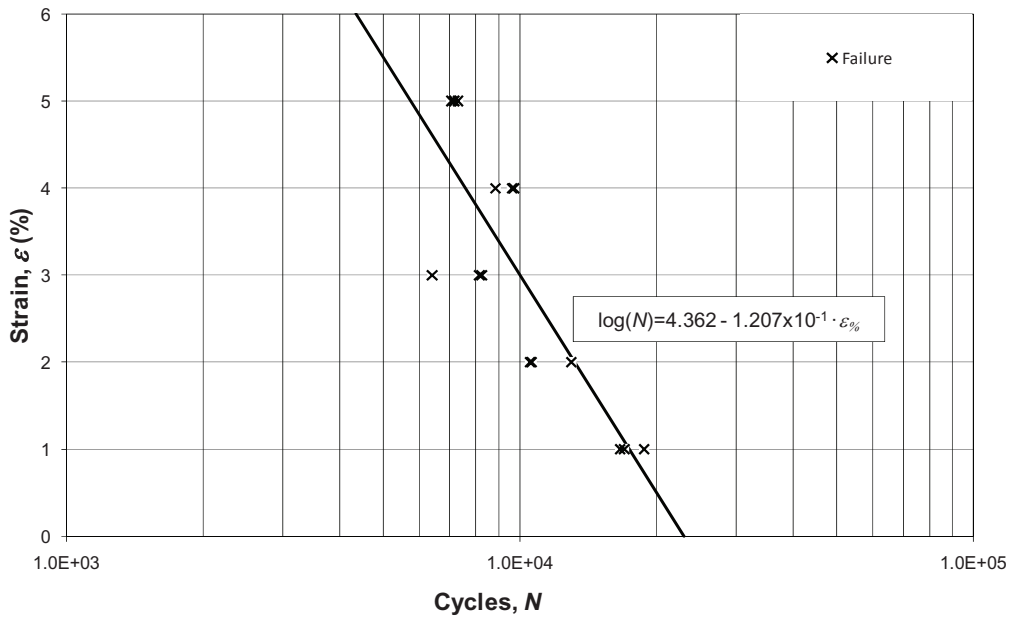

Fig. 10. Woehler's diagram with the fatigue results for the constant-strain test

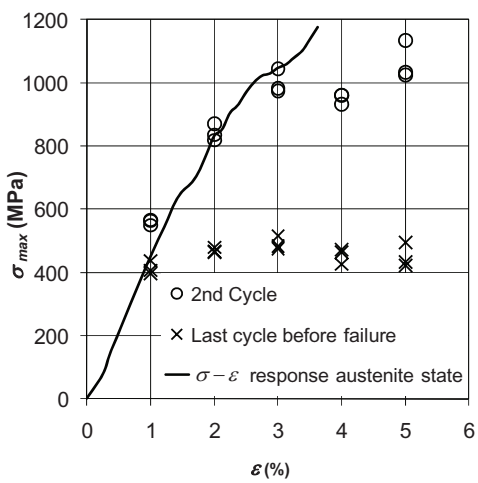

Fig. 11. Maximum stresses in the wire under constant-strain loading measured for different applied strains during: (a) the second cycle after test start; (b) the last cycle before test termination

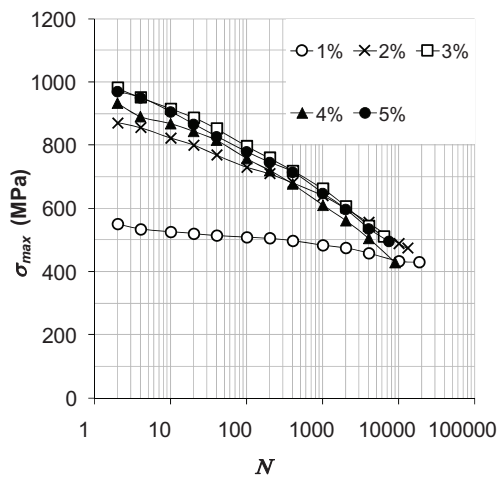

Fig. 12. Evolution of the maximum stress in the wire under constant-strain loading

4. Discussion

4.1. Constant-stress tests

Table 1 shows that the target of maximum stress oscillation ($\Delta\sigma$ within 6% of the nominal stress) was achieved for all specimens, indicating a good accuracy of the tests performed. Another important quality achievement was the occurrence of all failures in the free span of the wire samples with the fractures taking place at a distance never less than 10 mm from the grips. The very low scatter of the experimental points in Fig. 6 is also a remarkable

achievement given the prismatic shape and the very smooth surface of the wire samples sunder test (repeatability of fatigue lives are more common for highly notched specimens).

Figure 6 shows that the inclined part of Woehler's curve is reasonably well represented by a straight line. The slope of the interpolating line is rather flat, indicating that the fatigue life of the SMA wire decreases very quickly for increasing applied stress. From the equation of the inclined portion reported in Fig. 6, a slope $\sigma/\log(N_f) \approx 101$ MPa is calculated, a figure that correlates favourably with the slope of 117 MPa reported by Araujo et al. [9] for an alloy Ti.45.0Ni-5Cu(%at).

The fatigue limit calculated from Fig. 6 for the chosen life (5×10^5 cycles) is $\sigma_w = 101.8$ MPa, corresponding to a confidence level of 50%. The distribution of the experimental points in Fig. 6 along the horizontal part of the Woehler's curve suggests that the existence of a true fatigue limit of the material under constant-stress conditions is very likely. To verify this conclusion, the samples that survived the staircase method in Table 1 (specimens 3, 11 and 14) will be mounted on the machine and cycled again for several million cycles to see if any failure occurs.

It is worth noting that the life results under constant-stress reported by the manufacturer (SAES Getters) of the wire tested here are much higher than the life data displayed in Table 1. For example, the manufaturer's data sheet gives a life $N_f = 10^5$ cycles and a length drift of about 0.17% for an applied stress $\sigma = 170$ MPa. These results compare poorly with the present outcome, giving a life $N_f = 8\,710$ cycles (average of tests 1 and 7 in Table 1) and a drift of about 0.45% (Fig. 9b) under an applied stress $\sigma = 150$ MPa. This big difference can perhaps be explained by the difference in test conditions under which the fatigue data were obtained. Starting from the wire undergoing the maximum elongation in the martensitic state (low temperature), SAES Getters test conditions supply heat to the wire until a differential strain $SME = 3.5\%$ is achieved, testifying only a partial transformation of the alloy. In the present investigation, the alloy is transformed completely, giving for $\sigma = 150$ MPa a differential strain $SME \approx 4.4\%$ (Table 1, tests 1 and 7). The beneficial effects on the fatigue life associated to partial austenite transformation has been reported by several authors [5, 6] and could explain the difference in fatigue performance observed here. Exploring systematically the effect of partial transformation on the fatigue response of shape memory alloys undergoing constant-stress loading would be a fruitful research field to investigate.

The wire strains reported in Fig. 7a for the second test cycle show that both maximum (martensitic) and minimum (austenitic) strains increase almost linearly with the applied stress. This behaviour is coherent with the monotonic stress-strain curve of the alloy (Fig. 5a,b), which shows that in the range of applied stresses covered in Fig. 7a (100-200 MPa) both martensitic and austenitic stress-strain curves are fairly linear. As a consequence, also the differential strain (*SME* in Fig. 7a) increases almost linearly with the applied stress. The small increase in differential strains seen in Fig. 7a when the applied stress passes from $\sigma = 175$ MPa to $\sigma = 200$ MPa supports the conclusion by Bigeon and Morin [8] that the shape memory effect (measured by the differential strain *SME*) achieves a maximum in NiTi alloys for an applied stress around 200 MPa.

When the behaviour of the alloy after a considerable number of cycles is examined (Fig. 7b), a different strain pattern emerges. For the last cycle before test termination, Fig. 7b shows that the differential strain (*SME*) is lower than for the second cycle when the applied stress σ stays below 125 MPa. By contrast, the performance remains more or less stable (in comparison to the second cycle) for stresses $\sigma \geq 125$ MPa. Apparently, the shape memory alloy becomes less and less efficient as the material accumulates strain cycles under relatively low applied stresses.

This remark is confirmed by the strain evolution with the number of cycles plotted in Fig. 8. Figure 8a shows that for $\sigma = 100$ MPa the martensite strain is nearly constant across the cycles while the austenitic strain increases with the cycles so that the differential strain progressively decreases. From a functional point of view, this behaviour corresponds to a decrease of the austenitic Young's modulus as the cycles accumulates. For higher applied stresses ($\sigma \geq 125$ MPa), Fig. 8b,c,d show that martensite and austenite strains increase with the same rate over the cycles so that the differential strain *SME* remains unchanged.

For the sake of the actuator efficiency (high strokes) the above results would suggest using the SMA wire under relatively high backup stresses to maximize the differential strain *SME*. However, Fig. 9b shows that for high applied stresses ($\sigma \geq 125$ MPa) the length drift of the wire is considerable, indicating that the alloy accumulates permanent plastic strains as the cycles go on. The length drift (hence the permanent plastic strain) of the wire is much more contained for the lower stress levels ($\sigma \leq 100$ MPa) as shown in Fig. 9a. From a practical standpoint, a trade-off between the advantages (higher stroke) and disadvantages (high drift, hence poor repeatability) of the stress on the wire is to be found. Overall, the data from the present research suggest that a stress level of about

125 MPa would ensure appreciable differential strains (large actuator strokes) with acceptable length drift (less than 0.2% from Fig. 9b).

4.2. Constant-strain tests

Since the failures of all the samples tested under constant-strain conditions occurred outside the grips of the machine, the fatigue data in Table 2 are quite meaningful for the true response of the alloy. Table 2 shows that, irrespective of the strain applied, all samples failed after a relatively low number of cycles ($7\,000 < N_f < 19\,000$). This outcome confirms that the constant-strain loading condition is much more demanding on the material than the constant-stress test, even though the maximum strains induced in the alloy are of the same order of magnitude in the two tests.

Woehler's semi-log diagram in Fig. 10 shows that the fatigue points are reasonably well interpolated by a straight line. A small departure from the linear trend is represented by lives at 3% strain, which are lower than those at 4% strain, but these uncertainties are typical of the behaviour of most materials even under purely mechanical fatigue. The slope of the interpolating line in Fig. 10 is $\varepsilon/\ln(N) \approx 8.38$.

From Fig. 11 it is seen that the maximum stress induced in the wire during the second loading cycle (hollow circles) for each strain level is consistent with the monotonic stress-strain curve of the austenitic alloy (Fig. 5a). During the last cycle before failure (crosses in Fig. 11) the fatigue data fall quite below the monotonic stress-strain curve and failures occurs at a terminal stress between 400 and 500 MPa, regardless of the applied strain.

The departure of the stress-strain response from the monotonic curve for increasing cycles is confirmed by Fig 12, showing a progressive decrease of the maximum stress with the life. Since the trend of the interpolating curves in Fig. 12 is approximately linear in the semi-log chart, the stress decay is exponential. Although starting from very different maximum stresses at cycle 2, the curves in Fig. 12 terminate when the stress falls in the range 400-500 MPa. Dropping of the maximum stress into this range could be adopted as a predictor of incipient fracture of the material undergoing constant-strain functional cycling of whatever amplitude.

The constant-strain tests have shown that the shape memory wire under examination exhibits to some degree a two-way shape memory effect. This became clear in step 6 of the test procedure (see Section 2.5) when the wire loosened slightly between the grips after cooling down from the restraining step carried out in the (hot) austenitic state. This two-way shape memory effect, which tended to disappear over the cycles, could explain the peculiar trend of the wire drift detected in some constant-stress tests. For the lowest applied stresses ($\sigma = 89$ and 100 MPa) Fig. 9a shows that the drift decreases over the first cycles, denoting a shortening of the wire that could be due to the second memory of the material fading away.

5. Conclusions

Four types of tests are described to characterize the strength-life properties of shape memory wires under functional fatigue loading: constant-stress test, constant-strain test, constant-stress test with limited maximum strain, cyclic-stress test with controlled maximum strain. The tests are developed to be significant for most of the loading conditions occurring in real-life shape memory actuators. A test machine has been built capable of applying those test conditions and a test campaign on a commercial NiTi wires (SAES Getters Smartflex®) was carried out under constant-stress and constant-strain conditions.

The test results under constant-stress loading show that:

- the strength-life (Woehler's) curve on a semi-log diagram is similar to ordinary metals', with an initial inclined line followed by a final horizontal line. For the Smartflex® wire the inclined line has a slope $\sigma/\log(N_f) \approx 101$ MPa while the horizontal line identifies a fatigue limit (at 5×10^5 cycles) $\sigma_w \approx 102$ MPa;
- for applied stresses below the fatigue limit, the length drift of the wire is negligible (less than 1%) and the differential strain (shape memory effect) in the wire is acceptable for practical purposes;
- for applied stresses above the fatigue limit, the differential strain increases but is accompanied by greater and greater length drifts.

The test results under constant-strain loading show that:

- the strength-life (Woehler's) curve on a semi-log diagram features only the inclined part (the wire failed for all strain levels tested between 1 and 5%) and there is no indication of a strain threshold (strain fatigue limit);
- the functional life can be as low as 7 000 cycles (for applied strain of 5%) and never exceeds 19 000 cycles (applied strain of 1%) in the strain range investigated;
- the stress induced in the wire decreases exponentially with the number of cycles. The residual stress just before failure falls in the range 400-500 MPa, regardless of the strain applied.

In conclusion, NiTi shape memory wire should be used in actuators under loading conditions as close as possible to a constant-stress situation. Exposure to constant-strain conditions due to over-restraint of the wire or pseudo-restraint conditions promoted by dynamic loading is very detrimental to the fatigue life and should be avoided.

References

[1] Spinella I, Dragoni E. Design equations for binary shape memory actuators under dissipative forces. *Proceedings of the Institution of Mechanical Engineers, Part C: J. of Mechanical Engineering Science* 2009; **223**:531–543.

[2] G. Eggeler G, Hornbogen E, Yawny A, Heckmann A, Wagner M. Structural and functional fatigue of NiTi shape memory alloys. *Materials Science and Engineering A* 2004; **378**:24–33.

[3] Fumagalli L, Butera F., Coda A. SmartFlex NiTi Wires for Shape Memory Actuators. *J. of Materials Engineering and Performance* 2009; **18**:691–5.

[4] Mertmann M, Vergani G. Design and application of shape memory actuators. *Eur. Phys. J. Special Topics* 2008; **158**:221–230.

[5] Bertacchini OW, Lagoudas DC, Patoor E. Thermomechanical transformation fatigue of TiNiCu SMA actuators under a corrosive environment – Part I: Experimental results, *Int. J. of Fatigue*, 2009, **31**:1571–1578.

[6] Lagoudas DC, Miller DA, Rong L, Kumar PK. Thermomechanical fatigue of shape memory alloys. *Smart Materials and Structures* 2009; **18**:085021.

[7] Bigeon MJ, Morin M. Fatigue of the shape memory effect in thin wires-comparison between TiNi and CuZnAL. *J de physique IV* 1995; **C2**:385-390.

[8] Bigeon MJ, Morin M. Thermomechanical study of the stress assisted two way memory effect fatigue in TiNi and CuZnAl wires. *Scripta materialia* 1996; **35**:1373-8.

[9] Araujo CJ, Morin M, Guerin G. Fatigue behavior of Ti-Ni-Cu thin wires SME. *J. de physique IV France* 1997; **C5**:501-6.

[10] Mertmann M, Bracke A. Hornbogen E. Influence of the thermal treatment on the stability of partially constrained recovery of NiTi Actuator wire. *J. de physique IV* 1995; **C8**:1259-1264.

[11] Demers V, Brailovski V, Prokoshkinb SD, Inaekyana KE. Thermomechanical fatigue of nanostructured Ti–Ni shape memory alloys. *Materials Science and Engineering A* 2009; **513-514**:185-196.

[12] Zanotti C, Giuliani P, Tuissi A, Arnaboldi S, Casati R. Response of NiTi SMA wire electrically heates. *Esomat* 2009; **06037** DOI:10.1051/esomat/200906037.

[13] Nakazawa H, Kodama S. Statistical S-N testing method with 14 specimens: JSME standard method for determination of S-N curves. *Statistical research on fatigue and fracture* 1987:59–69.